COVER SHEET

Title: **PELE Fragmentation Dynamics**

Authors : J. Verreault
N. van Hinsberg
E. Abadjieva

Paper ID: 13519887

TNO, Lange Kleiweg 137, P.O.Box 45, Rijswijk, 2288 GJ, The Netherlands

(FIRST PAGE OF ARTICLE)

An analytical model that describes the PELE fragmentation dynamics is presented and compared with experimental results from literature. The model accounts for strong shock effects and detailed interactions taking place between the filling – the inner core of the ammunition – and the target (including shock wave, expansion wave, free surface and interface interactions). This model is also compared with a simplified model that uses the acoustic approximation and neglects the different wave interactions, which was employed by previously published PELE analytical models. The results are compared quantitatively in terms of fragments' radial velocities and qualitatively in terms of number of fragments, their mass distribution and the fragmentation length of the jacket. It is shown that strong shock effects and detailed wave interactions must be accounted for in order to simulate accurately the pressure evolution in the filling, which is the origin of the fragmentation dynamics, especially for impact velocities beyond 1000 m/s.

I. INTRODUCTION

A special type of ammunition, the Penetrator with Enhanced Lateral Efficiency (PELE), was developed and experimentally investigated at *Institut Saint-Louis* (ISL) during the period from 1996 to 2004. From this investigation, it was observed that downstream of the impact with a target plate, the PELE fragments expanded laterally at a larger extent than for a more conventional type of ammunition, resulting in a larger damaged surface area behind the target.

PELE ammunitions are composed of two parts: a jacket and a filling. The jacket is a cylindrical tube made from a relatively dense and brittle material (e.g. tungsten or steel). The filling is inserted inside the jacket and is made of a less dense material (e.g. aluminum or polyethylene). Upon impact, shock waves propagate in both parts. The PELE effect originates from the fact that the Poisson's ratio of the filling is larger than that of the jacket. Consequently, as both parts are compressed by shock waves, the radial expansion of the jacket is less than that of the filling. However, since both parts interact with each other, a radial stress is created. The radial stress causes a hoop stress in the jacket that can exceed the ultimate strength of the jacket material. When this occurs, the jacket fails, fragments are generated and accelerated radially.

Paulus and Schirm [1] reported experimental measurements of PELE fragmentation behind a target plate. They varied the impact velocity between 900 and 3000 m/s for different filling and target materials. From X-ray photography, the radial velocity of the fragments was measured. The photographs also provided a qualitative indication of the fragmentation pattern in terms of size distribution and number of fragments. In their study, Paulus and Schirm also included an analytical approach to predict the performance of PELE ammunition. In their model the acoustic wave approximation was used to calculate the pressure evolution in the filling, which was in turn used to calculate the radial acceleration of the fragments. This approximation implied that compression and expansion waves travel at a constant velocity for all impact conditions. Jiansheng [2] conducted an experimental, numerical and theoretical study on the PELE phenomenon. Although the analytical approach accounted for additional aspects (such as shear stresses), the acoustic approximation was also used as a basis for their model.

The acoustic wave approximation is valid for relatively low impact velocities. For higher impact velocities, the discrepancy between the acoustic model and the reality increases. The purpose of this study is to incorporate strong shock effects and detailed interactions into an analytical PELE fragmentation model. This is achieved by using shock Hugoniot data for the considered materials in order to calculate the evolution of the material properties and by accounting for detailed interactions between shock waves, expansion waves, free surfaces and interfaces. A comparison between the results obtained from such an analysis, those provided by the acoustic approximation and the experimental results provided by Paulus and Schirm are presented in this work.

II. DESCRIPTION OF THE ANALYTICAL MODEL

The ideal analytical model to describe the PELE fragmentation dynamics would be capable of predicting the number of fragments generated, their mass and size distribution and the velocity components for each fragment. In order to approach this ideal model, the pressure evolution in the filling and the radial expansion of the jacket must be simulated accurately for all axial positions along the projectile. A schematic of the wave propagation in the projectile and the target shortly after impact is shown in Figure 1 (where half of the projectile is shown). The wave propagation is illustrated qualitatively to show the different types of waves that influence the PELE fragmentation mechanism. Material deformation and fragmentation is not shown for simplicity. In this figure, the shock wave in the filling propagates faster than in the jacket. This is representative, for instance, of an aluminum filling and a tungsten jacket. Behind the shock wave that propagates in the jacket, the material is free to expand radially and a radial expansion wave propagates towards the axis of symmetry (see Figure 1b). In the target, the shock wave reflects as an axial expansion wave upon the interaction with the back surface (see Figure 1b). A certain amount of time is required before any of the two expansion waves enters the filling to release the pressure. It is during this time that the filling exerts a radial stress on the jacket and causes a radial expansion. It is therefore important to model as accurately as possible the pressure evolution in the filling.

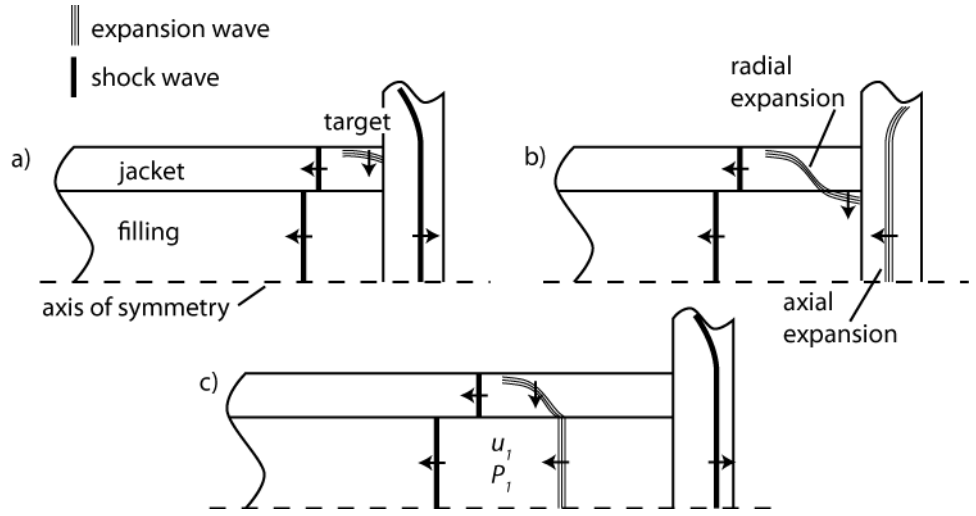

Figure 1. Schematic of the shock and expansion waves involved in an impact between a PELE ammunition and a target plate.

Three submodels are presented in the next subsections: the acoustic, the shock and the fragmentation submodels. The complete PELE analytical model consists of the acoustic *or* shock submodel (depending on whether the acoustic approximation is used) *and* the fragmentation submodel.

Acoustic Submodel

Denoting the particle velocity as u, the projectile impact velocity as u_o, the sound speed as c, the pressure as P and the density as ρ, the shock / expansion wave velocity and the particle pressure are expressed as:

$$U_s = c \tag{1}$$

$$P = \rho c(u_o - u) = Z(u_o - u) \tag{2}$$

where Z is the material acoustic impedance. After impact, the particle velocity and pressure must be equal across the interface between the filling (subscript f) and the target (subscript t). Using Eq. 2 for the filling and the target, the following relations are obtained for the pressure and the particle velocity behind the shock waves in the filling and target:

$$P = u_o \frac{Z_f Z_t}{Z_f + Z_t} \qquad u = u_o \frac{Z_f}{Z_f + Z_t} \tag{3}$$

The radial expansion wave propagates at $U = c_j$ from time $t = 0^+$ after the time of impact and the axial expansion wave propagates at $U = c_t$ from time $t = h_t / c_t$, where h_t is the target thickness. Behind both expansion waves, the pressure is zero. The first expansion wave to enter the filling determines the time at which the pressure is released $t_{p=0}$. In the filling, the relative velocity between the shock and expansion waves is $u_o - u_1$, where u_1 is the particle velocity behind the shock wave in the laboratory frame of reference (see Figure 1c). Therefore, the expansion wave interacts with the shock wave at time $t = t_{p=0}\,(u_o - c_f) / (u_o - u_1)$.

Shock Submodel

In the shock submodel, uniaxial strain is assumed for the filling. This assumption is generally employed to describe wave propagation in flyer plates impacting a target where the edge effects can be neglected (which is valid near the center of the plate). The uniaxial strain assumption is also valid for the filling in a PELE ammunition since it is constrained by the jacket during the timeframe of interest (before significant radial expansion occurs).

The shock wave – particle velocity relation is expressed as:

$$U_s = c + su \tag{4}$$

and the pressure – particle velocity equation is:

$$P = \rho c(u_o - u) + \rho s(u_o - u)^2 \tag{5}$$

Using this equation for a filling that impacts a target, the pressure and particle velocity is obtained across the interface. The density is then derived using the conservation of mass. The shock velocity in each material is calculated using Eq. 4.

Other wave interactions considered in the shock submodel are: the target shock wave – free surface interaction (between Figures 1a and 1b), the target expansion wave – interface interaction (between Figures 1b and 1c) and the filling expansion wave – filling shock wave interaction (after Figure 1c). A description of these wave interactions is given by Cooper [3]. For the situation where the target impedance is larger than that of the filling (e.g. for an aluminum filling and a steel target), the interaction between the target expansion wave and the interface results in an expansion wave propagating in the filling and a shock wave propagating in the target (see Figure 1c). In this case, the pressure behind the filling expansion wave is lower than P_1, but larger than zero (as opposed to the acoustic submodel). The pressure in the filling is completely released behind the radial expansion wave. An example of the complete wave interaction between the filling and the target is provided in Section IV.

Fragmentation Submodel

The acoustic or shock submodel provides the pressure (or axial stress σ_x) evolution in the filling. The corresponding radial stress between the filling and the jacket is:

$$\sigma_r(t) = \frac{\nu_f}{1 - \nu_f}\sigma_x(t) - \varepsilon_{r,f}(t)E_f \tag{6}$$

where ν_f and E_f are the Poisson's ratio and the Young modulus of the filling material, respectively, and $\varepsilon_r(t) = (r(t)_f - r_{o,f}) / r_{o,f}$ is the radial strain of the filling which increases only if the jacket fails. Failure of the jacket occurs if the hoop stress (caused by the radial stress) exceeds the ultimate strength of the jacket material. Using the thin shell approximation, the condition for the jacket failure is:

$$\sigma_h(t) = \frac{\sigma_r(t) r_j}{h_j} > \sigma_{ult} \tag{7}$$

where r_j and h_j are the mean radius and the thickness of the jacket, respectively. The acceleration of the jacket fragments is given by the law of motion:

$$a_j(t) = \frac{\sigma_r(t) A_j}{m_j} \tag{8}$$

where A_j is the inner surface area of the jacket and m is the total mass of the accelerating fragments. Acceleration continues until the filling reaches its radial strain limit given by:

$$\varepsilon_{r,lim}(t) = \frac{\nu_f \sigma_x(t)}{(1-\nu_f)E_f} \tag{9}$$

Once this strain limit has been reached, the fragments keep a constant radial velocity.

The fragmentation submodel uses the procedure suggested by Mott [4] with an additional formula obtained from Gold and Baker [5]. Figure 2 presents a schematic to illustrate the procedure adopted for the fragmentation of the jacket. The following steps describe this procedure:

1 The expansion rate of the jacket $\dot{\varepsilon}_i$ is provided from Eq. 8.

2 The length of each fragment l_j and the total number of fragments for the considered ring N_i is determined statistically from 100 simulations of the Mott fragmentation procedure [4].

3 The averaged mass of the N_i fragments is given by the following expression [5]:

$$m_{avg,i} = \sqrt{\frac{2}{\rho}} \left(\frac{\sigma_{fr}}{\gamma_M}\right)^{3/2} \left(\frac{1}{\dot{\varepsilon}_i}\right)^3 \tag{10}$$

where σ_{fr} is the fracture stress and γ_M is the Mott constant. The mass of the ring is the sum of the fragment mass: $m_i = N_i\, m_{avg,i}$.

4 The length of the ring L_i is obtained geometrically using its mass, density and cross-sectional area.

5 Steps 1 to 4 are repeated for the next ring using the proper local value for the expansion rate $\dot{\varepsilon}_i$.

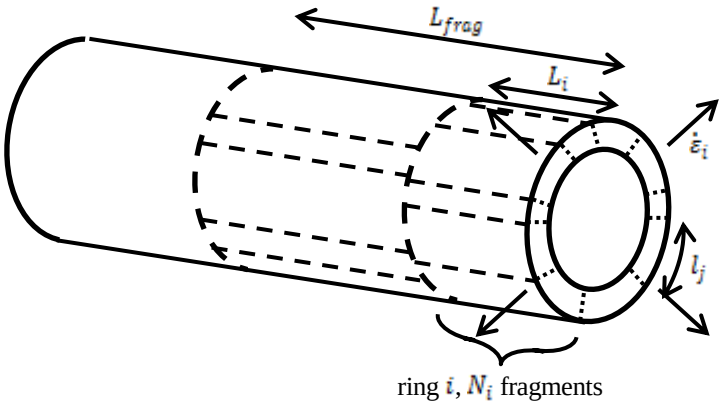

Figure 2. Schematic of the fragmentation procedure.

There are a few differences between the analytical model derived by Paulus and Schirm and the submodels presented herein. Table I presents the differences related to the calculation of the pressure evolution in the filling. The acoustic submodel has the same feature as the Paulus and Schirm model, except for the inclusion of the radial expansion wave. Table II shows the differences related to the fragmentation of the jacket. In Paulus and Schirm model, the radial stress is calculated from the axial and hoop stresses (neglecting the Poisson's ratio). The radial acceleration of the jacket occurs as long as the radial strain is smaller than the maximum elongation and the failure criterion is based on this parameter. Therefore, their model is substantially different than the fragmentation submodel.

TABLE I. COMPARISON BETWEEN THE PAULUS AND SCHIRM'S ANALYTICAL MODEL, THE ACOUSTIC AND THE SHOCK SUBMODELS

	Paulus and Shirm's analytical model	**Acoustic submodel**	**Shock submodel**
Wave velocity	c	c	$c + su$
Impact pressure	Eq. 3	Eq. 3	Eq. 5
Wave interaction	no	no	yes
Radial expansion wave	no	yes	yes

TABLE II. COMPARISON BETWEEN THE PAULUS AND SCHIRM'S ANALYTICAL MODEL AND THE FRAGMENTATION SUBMODEL

	Paulus and Shirm's analytical model	**Fragmentation submodel**
Radial stress	σ_x - σ_h	Eq. 6
End of radial acceleration	$\varepsilon_r = \varepsilon_{j,max\ elongation}$	Eq. 9
Jacket failure criterion	$\varepsilon_r > \varepsilon_{j,max\ elongation}$	$\sigma_h > \sigma_{ult}$
Fragmentation	no	Mott + Gold and Backer

III. IMPACT CONDITIONS

The PELE fragmentation model described in this work is compared with the experimental results of Paulus and Schirm [1]. They used 80 mm-long projectiles with jacket inner and outer radii of 3 and 5 mm, respectively. The projectiles were shot from a smooth-bore launcher. The remaining impact conditions for the reported cases are provided in Table III. The material properties necessary for the analytical submodels are included in Table IV.

TABLE III. EXPERIMENTAL CONDITIONS FROM PAULUS AND SCHIRM [1]

Case	**Filling material**	**Target material**	**Target thickness (mm)**	**Impact velocity (m/s)**
1	A-G3	A-U4G	3	929 / 1275 / 2457
2	A-G3	A-U4G	8	937 / 1254 / 2472 / 2984
3	A-G3	XC 48	3	925 / 1261 / 2441
4	PE	A-U4G	3	924 / 1279 / 2420
5	PE	A-U4G	8	939 / 1258 / 2445 / 2977
6	PE	XC 48	3	936 / 1262 / 2475

TABLE IV. MATERIAL PROPERTIES

Property	**A-G3 (aluminum)**	**A-U4G (aluminum)**	**PE (polyethylene)**	**D 180 K (tungsten)**	**XC 48 (steel)**
Density (g/cm^3)	2.65	2.8	0.92	18	7.823
E (Pa)	74E9	74E9	2.4E9	360E9	201E9
σ_u (Pa)	———	———	———	680E6	———
v	0.35	0.35	0.46	———	———
c (m/s)	5176	5106	2187	4029	4797
s	1.35	1.35	1.481	1.237	1.49

IV. RESULTS

Before comparing the radial velocities of the fragments and the fragmentation patterns, a typical calculation is described in detail by considering Case 4 from Table III with an impact velocity of 1279 m/s.

Typical calculation (Case 4, u_o = 1279 m/s)

A common method to calculate the impact pressure across the filling – target interface is to plot their Hugoniot on a P–u plane using Eq. 5 (or Eq. 3 when using the acoustic approximation). This is illustrated in Figure 3 for both the acoustic and shock submodels. The impact pressure is obtained at the intersection of both materials' Hugoniot. For the acoustic submodel, the impact pressure is approximately 2.3 GPa, which is significantly lower than that for the shock submodel (3.6 GPa). This difference is mainly due to the quadratic dependence of the filling Hugoniot (i.e. due to the strong shock effect).

Within a few tens of microseconds after the impact, shock and expansion waves propagate in the filling and the target. Figure 4 illustrates the complete wave interactions taking place, except for the radial expansion wave. The dash lines are the particle trajectories of the filling. At time $t = 0$ the filling and the target are located at $-0.08\ \text{m} < x < 0\ \text{m}$ and $0\ \text{m} < x < 0.003\ \text{m}$, respectively. At $t > 0$, shock waves propagate in the filling and the target. The target shock wave reflects as an expansion wave upon interaction with the free surface at t_1. The expansion wave enters the filling and interacts with the filling shock wave at t_2. The filling shock is weakened and decelerated by the expansion wave. In the target, there are repeated cycles consisting of a shock wave formed at the interface that reflects as an expansion wave at the free surface. At $t = 28\ \mu\text{s}$ the filling shock wave reaches the back of the filling. In the shock submodel, the interactions that follow are not considered, since the most influential timeframe for the PELE fragmentation dynamics occurs before the shock wave reaches the back of the filling.

The shock submodel provides the pressure evolution for all the particles in the filling. This is illustrated in Figure 5 for the particles at initial locations $x = 0$ m and $x = -0.04$ m. In this figure, the profile of the shock submodel (without radial expansion wave) corresponds to the wave interactions displayed in Figure 4. The profile that accounts for the radial expansion wave is shown with the dashed line. The profiles with and without the radial expansion wave are the same in the time range $0 < t < t_1$. At t_1 the radial expansion wave enters the filling and completely releases the

pressure. In this figure, the pressure evolution provided by the acoustic submodel is also illustrated with the dash-dot line.

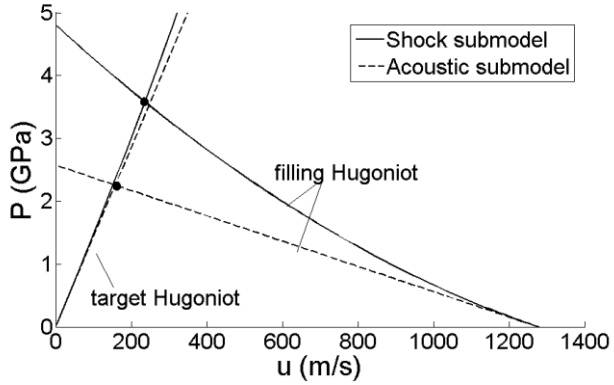

Figure 3. Filling and target Hugoniots for Case 4 with an impact velocity of 1279 m/s.

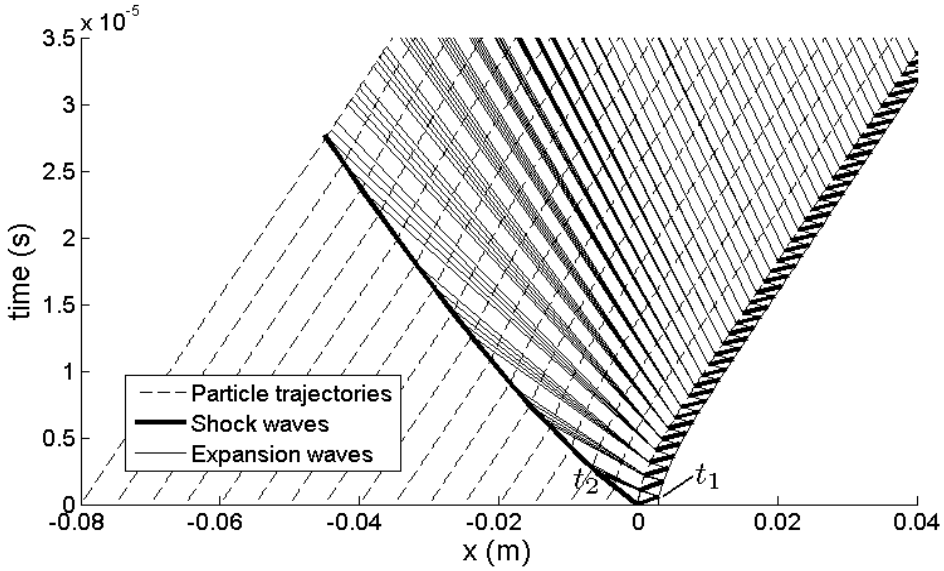

Figure 4. Wave interaction taking place in the filling and the target for Case 4 with an impact velocity of 1279 m/s.

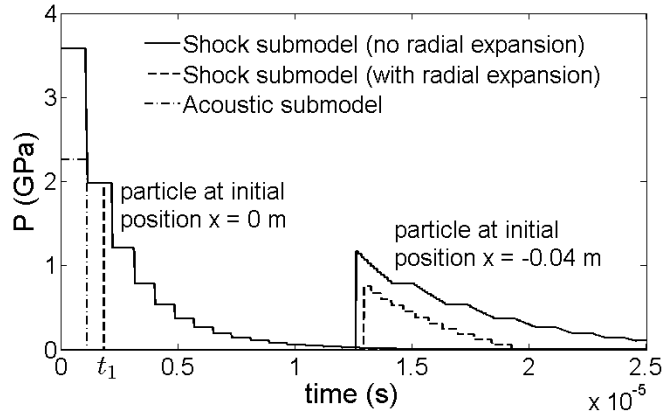

Figure 5. Pressure evolution for the particles initially at 0 and –0.04 m for Case 4 with an impact velocity of 1279 m/s.

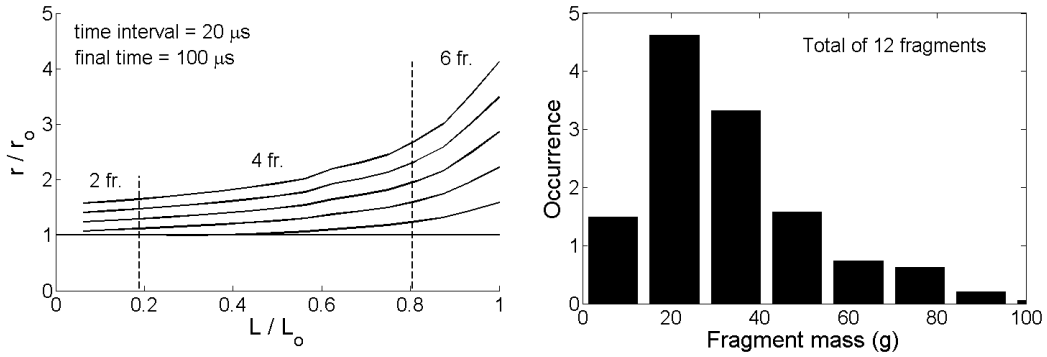

Figure 6. Fragments' radial position and mass distribution for Case 4 with an impact velocity of 1279 m/s.

The hoop stress in the jacket caused by the filling particles initially at x_o = –0.075 m and x = 0 m is in this case 0.73 and 5.9 GPa, respectively, immediately after the particles cross the filling shock wave. Since the ultimate strength for tungsten is 0.68 GPa, fragmentation of the complete jacket length occurs. A visualization of the fragments radial acceleration is presented on the left-hand side of Figure 6. Each line corresponds to the radial position of the fragments at a specific time. The time interval between each line is 20 μs. The final radial velocity of the fragments at L / L_o = 1 is 127 m/s. The fragmentation submodel predicts 6 fragments with a length of approximately L / L_o = 0.2 at the front of the projectile followed by 4 fragments with a length of approximately L / L_o = 0.62. The mass distribution of all the fragments is shown on the right-hand side of Figure 6.

Fragments Radial Velocity (Cases 1 to 6)

The maximum radial velocity of the fragments calculated with the acoustic and shock submodels (accounting for the radial expansion waves) is shown in Figure 7. Figures 7a to 7c correspond to an aluminum filling (Cases 1 to 3). In general, the shock submodel provides slightly lower radial velocities than the experimental values. However, the shock submodel predicts well the trend, except for an impact velocity of 3 km/s in Figure 7b. The acoustic submodel provides lower radial velocities in all cases. The difference increases for increasing impact velocity. Simulations with a polyethylene filling are illustrated in Figures 7d to 7f (corresponding to Cases 4 to 6). The trend of the simulation reproduces well that of the experimental results, although the results from the shock submodel are slightly higher than the experimental values.

Fragmentation (Case 6)

Comparison of the fragmentation pattern calculated from the analytical model (using the shock and fragmentation submodels) and the experimental results can be made qualitatively, since no data was provided by Paulus and Schirm [1] concerning the total number of fragments and their mass distribution. Figure 8 presents the comparison of the fragmentation for Case 6 with an impact velocity of 936 m/s. The experimental x-ray photograph was taken from their publication [1]. The time at

which the photographs were taken was not mentioned. The analytical model predicts a total of 9 fragments with most of them weighing between 5 and 17 g.

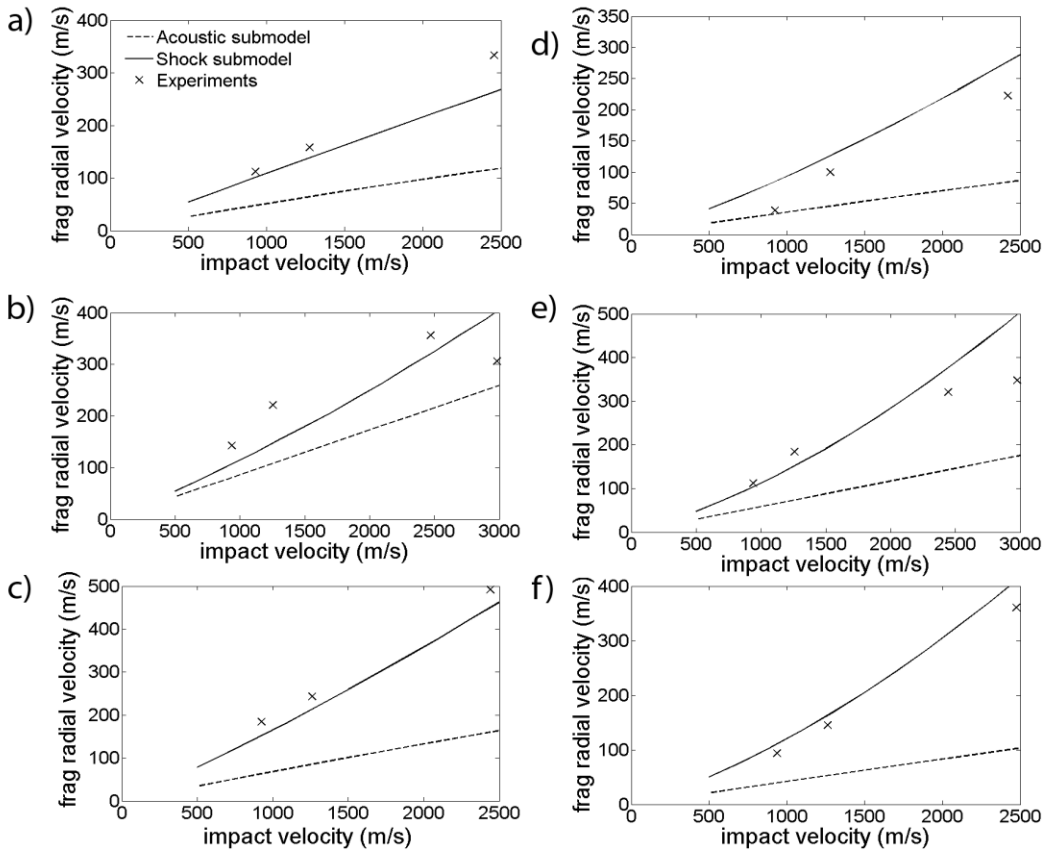

Figure 7. Fragments' maximum radial velocity. Figures a to f corresponds to Cases 1 to 6, respectively. Experimental values are given by Paulus and Schirm [1].

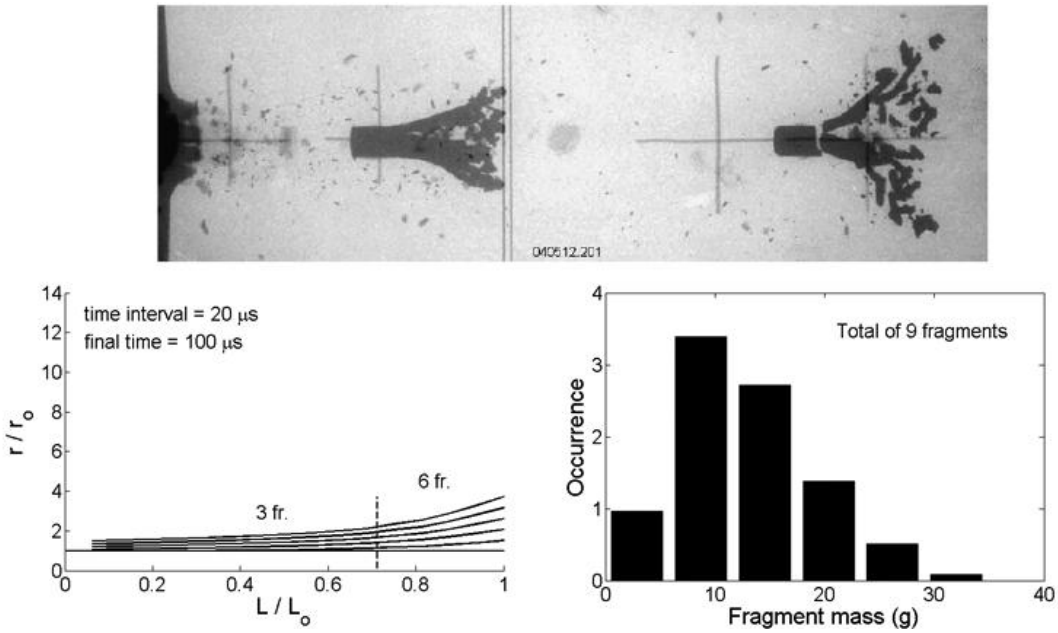

Figure 8. X-ray photograph, radial position of the fragments and their mass distribution for Case 6 with an impact velocity of 936 m/s. The x-ray photograph is given by Paulus and Schirm [1].

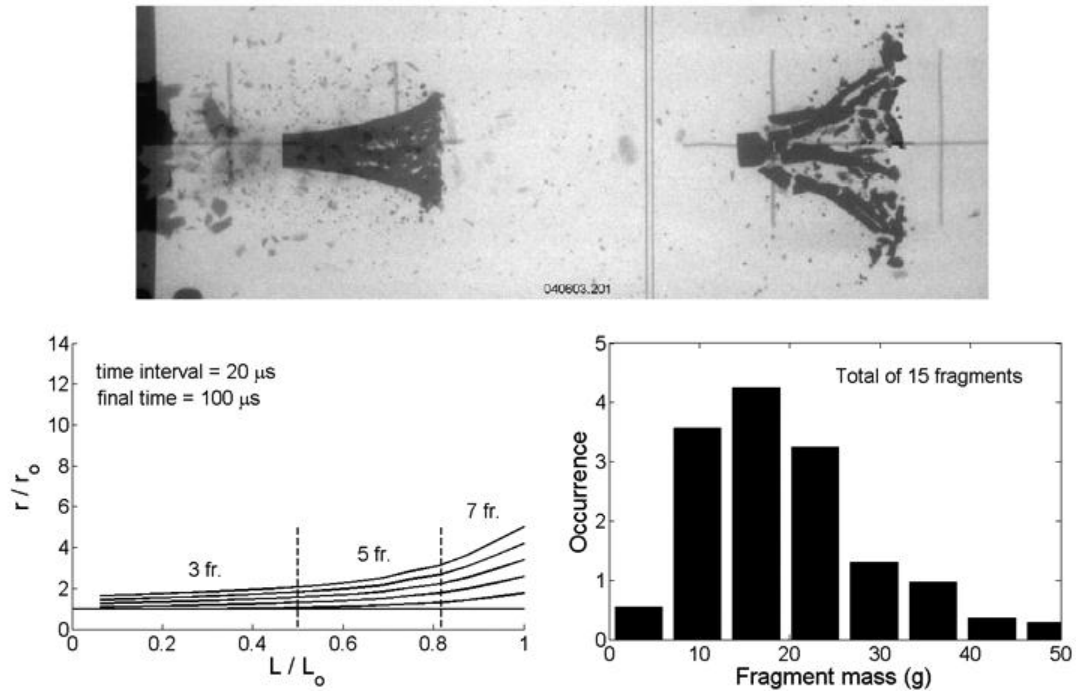

Figure 9. X-ray photograph, radial position of the fragments and their mass distribution for Case 6 with an impact velocity of 1262 m/s. The x-ray photograph is given by Paulus and Schirm [1].

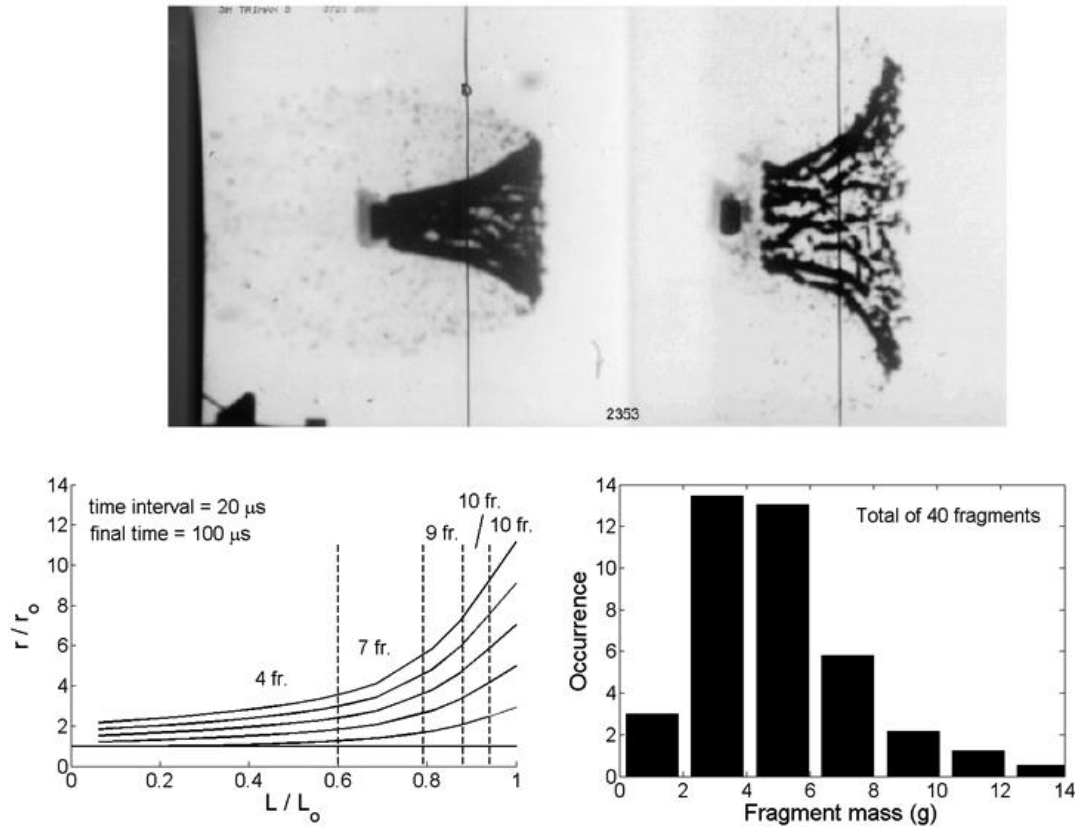

Figure 10. X-ray photograph, radial position of the fragments and their mass distribution for Case 6 with an impact velocity of 2475 m/s. The x-ray photograph is given by Paulus and Schirm [1].

Figures 9 and 10 show the results for Case 6 with an impact velocity of 1262 and 2475 m/s, respectively. As the impact velocity increases, the fragments' radial velocity increases, the number of fragments generated increases and their average mass decreases. For the highest impact velocity (Figure 10), a total of 40 fragments is predicted and the average mass is between 2 and 6 g. These results agree qualitatively well with the observations from the x-ray photographs. It can be observed from these photographs that at higher impact velocity (Figure 10), there are more fragments and they are on average smaller (therefore lighter) than at lower impact velocity (Figure 8). The radial position of the fragments along the projectile calculated from the analytical model also agrees qualitatively well with the experimental photographs.

IV. DISCUSSION AND CONCLUSIONS

An analytical model describing the fragmentation of PELE ammunitions behind a target plate was presented. This model was compared with experimental results and with a simplified model that used the acoustic approximation and neglected wave interactions. Both analytical models accounted for radial expansion waves created at the outer surface of the jacket. The fragments' radial velocities obtained from the shock submodel agreed well with the experimental results, whereas the acoustic submodel significantly underestimated the radial velocities, especially for impact velocities larger than 1000 m/s. This was due to the fact that the acoustic approximation underestimated the impact pressure (which reduced the radial force that accelerated the fragments) and neglected wave interactions (which provided a sudden pressure release in the filling as opposed to a stepwise pressure decrease). The shock submodel provided the pressure evolution of all filling particles, allowing the calculation of the fragmentation of the jacket at all axial positions. For increasing impact velocity, the number of fragments increased, whereas their mass and size decreased. This trend agreed well with the experimental X-ray photographs.

In conclusion, it was shown that in order to simulate accurately the pressure evolution in the filling and the radial acceleration of the fragments, it is important to incorporate the strong shock effects and detailed wave interactions in the PELE analytical model. In order to quantitatively validate the fragmentation model, additional experiments that provide the number of fragments and their mass are currently conducted.

V. REFERENCES

1. Paulus, G. and V. Schirm. 2006. "Impact Behavior of PELE Projectiles Perforating Thin Target Plates," *Int. J. Impact Eng.*, 33:566-279.
2. Jiansheng, Z. 2008. "Functional Mechanism of Penetrator with Enhanced Lateral Effect," PhD. thesis., Nanjing University of Science and Technology.
3. Cooper, P. W. 1996. "Explosives Engineering," Wiley-VCH, pp. 167-273.
4. Mott, N. F. 1947. "Fragmentation of Shell Cases," *P. R. Soc. London*, 189:300-308.
5. Gold, V. M. and R. L. Baker. 2008. "A Model for Fracture of Explosively Driven Metal Shells," *Eng. Fract. Mech.*, 75:275-289.